AD 718046

AD

AMMRC CR 70-20

DETERMINATION OF FLAWS IN AN 81 MILLIMETER PROJECTILE BODY USING THE TRW ACOUSTO-OPTICAL IMAGING DEVICE

August 1970

Robert Aprahamian

Applied Mechanics Laboratory
TRW SYSTEMS GROUP
One Space Park
Redondo Beach, California

DDC
FEB 9 1971
B

FINAL REPORT - CONTRACT DAAG46-70-C-0043

This document has been approved for public release and sale; its distribution is unlimited.

NATIONAL TECHNICAL
INFORMATION SERVICE

Prepared for

ARMY MATERIALS AND MECHANICS RESEARCH CENTER
Watertown, Massachusetts 02172

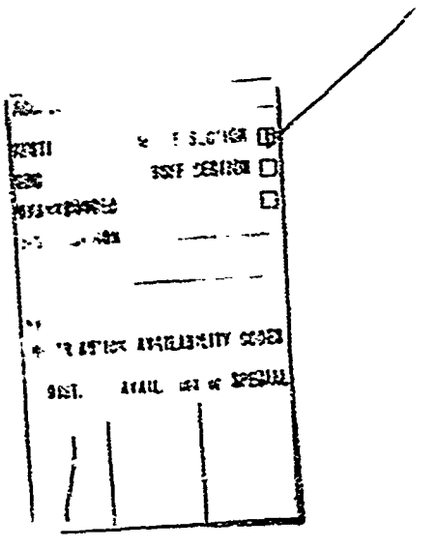

The findings in this report are not to be construed as an official Department of the Army position, unless so designated by other authorized documents.

Mention of any trade names or manufacturers in this report shall not be construed as advertising nor as an official indorsement or approval of such products or companies by the United States Government.

DISPOSITION INSTRUCTIONS

Destroy this report when it is no longer needed.
Do not return it to the originator.

AMMRC CR 70-20

DETERMINATION OF FLAWS IN AN 81 MILLIMETER PROJECTILE BODY USING THE TRW ACOUSTO-OPTICAL IMAGING DEVICE

Robert Abrahamian

Applied Mechanics Laboratory
TRW SYSTEMS GROUP
One Space Park
Redondo Beach

August 1970

Final Report - Contract DAAG46-70-C-0043

AMCMS Code PEMA 4931 0M 5042
Materials Testing Technology

This document has been approved for public release and sale; its distribution is unlimited.

Prepared for

ARMY MATERIALS AND MECHANICS RESEARCH CENTER
Watertown, Massachusetts 02172

ARMY MATERIALS AND MECHANICS RESEARCH CENTER

DETERMINATION OF FLAWS IN AN 81 MILLIMETER PROJECTILE BODY USING THE TRW ACOUSTO-OPTICAL IMAGING DEVICE

ABSTRACT

This report contains the results of a six month study designed to establish the applicability of the TRW Acousto-Optical Imaging System in depicting internal defects and surface flaws existing in an 81mm projectile body. An 81mm projectile body was furnished to TRW Systems which contained three known flaws. The known flaws consisted of two surface flaws on the outer surface of the shell and one crack in the inner wall. Acousto-optical images of these three flaws were obtained in the frequency range from 8 to 20 megacycles.

FOREWORD

This is the final report covering the work performed by TRW Systems Group from 30 January to 30 July 1970 on contract DAAG46-70-C-0043. The study reported herein was supported by the Army Materials & Mechanics Research Center, Watertown, Massachusetts. Mr. R. H. Brockelman served as Technical Supervisor of this program.

This project has been accomplished as part of the U. S. Army Materials Testing Technology Program, which has as its objective the timely establishment of manufacturing processes, techniques or equipment to insure the efficient production of current or future defense programs.

CONTENTS

INTRODUCTION

This program was initiated to determine the applicability of TRW's Acousto-Optical Imaging System in depicting flaws in projectile body casings. The Acousto-Optical Imaging Device has been successfully shown to provide an improved method of nondestructive testing having several advantages over competing techniques. The device uses ultrasonic probing waves to "look" into optically opaque objects. By exploiting the interaction between light and sound waves in a Bragg cell, an optical image of the flaw and/or defect is obtained on a real-time basis. The technique not only allows one to locate the defect but it also permits one to quantitatively assess the extent or size of the flaw. One of the principal features of the TRW acousto-optical nondestructive testing device is that it eliminates the need for a receiving transducer. The device may be operated at frequencies ranging from a few MHz to potentially hundreds of MHz. In the latter case a very high degree of resolution (~1 mil) can be obtained.

For ease in handling it was decided to initiate the program with an 81mm projectile containing defects rather than larger shells such as those of the 155mm class. The 81mm shell was supplied to TRW by the Army Materials and Mechanics Research Center. The shell contained three known flaws. Two flaws were on the outer surface of the shell and the third was a crack in the inner wall. The surface flaws are readily visible to the naked eye; the crack is not.

The three flaws existing in the 81mm shell were imaged using acoustic frequencies from 8 to 20 MHz. In each case, the known flaws were successfully imaged with sufficient resolution to specify their size and shape. Thus the device has been shown to be suitable for inspecting 81mm shells. Based on our experience with and understanding of the operation of the system, we can state with assurance that it can be used for the inspection of shells of larger caliber, for example, 155mm. We therefore suggest that a second phase of this program be initiated for the inspection of 155mm shells. Alternatively, a production type acousto-optical imaging system could be delivered to the Army Materials and Mechanics Research Center. The rest of this report provides a background of the acousto-optical imaging technique, a description of the shell which was used, the test procedure, test results and conclusions.

THEORETICAL BASIS FOR ACOUSTO-OPTICAL IMAGING

Background

The interaction of light and sound was postulated in 1922 by Brillouin.[1] He reasoned that since a train of acoustic waves represent cyclic regions of relative compression and relief a situation very similar to a common optical diffraction grating would exist. Perhaps due to the lack of proper instrumentation, experimental verification did not occur

until 1932 when Sears and Debye[2] succeeded in demonstrating the phenomenon. The immediate applications of Brillouin scattering, as the phenomenon has become known, lie in the area of determining the elastic properties of liquid materials. Many research papers (e.g., Ref. 3) were written relating critical parameters such as acoustic power density, the amplitude and wave length of light, and of more concern to use here, the angle at which the light wave interacts with the acoustic waves and the distance over which the light and sound waves interact. We will see that these two parameters have a pronounced effect on Acousto-Optical Imaging.

Interaction of Light and Sound

In order to fully describe the interaction of light with sound, one must understand the mechanical properties of sound. Simply stated, a train of sound waves is comprised of cyclic regions of relative compression and relief. Over the distance of one acoustic wavelength, Λ, the material supporting the acoustic wave experiences a change of pressure, P, density, ρ, and index of refraction, n, ranging from a maximum to a minimum and back again to a maximum as depicted in Figure 1 for a plane acoustic wave.

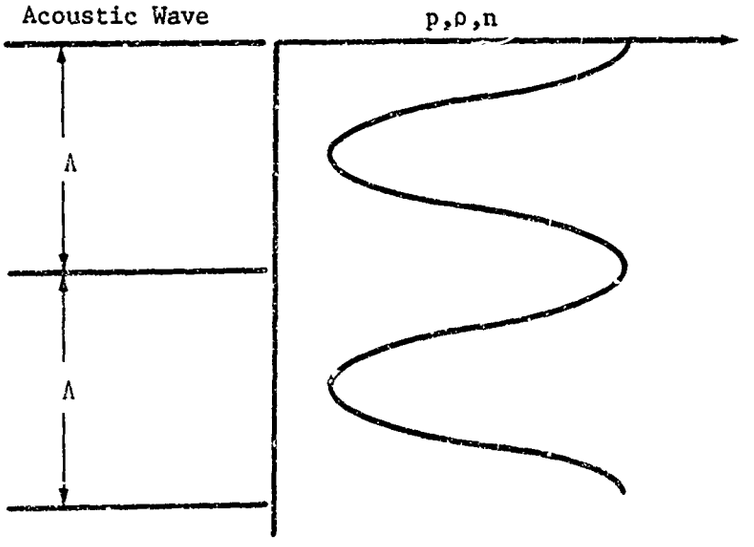

Figure 1. Pressure, density and index of refraction distribution as a function of position for a plane acoustic wave train of wave length Λ.

Sears-Debye Condition

Consider now a set of plane monochromatic light waves impinging an acoustic column of width, d. Since the velocity of light, c, depends on the index of refraction of the medium in which it is propagating according to

$$c = \frac{c_o}{n} \tag{1}$$

where c_o is the speed of light in vacuo, and n the index of refraction, the light will experience a time delay and a phase shift as it propagates through the acoustic wave column. As a consequence of the refraction being a function of position in the acoustic wave train and the fact that the acoustic wave is moving, each point in the material experiences a cyclic time variation of its index of refraction. As a result, the incident light becomes modulated in phase and also in frequency. It can be shown that if the acoustic column is sufficiently narrow, a carrier wave having the frequency of the incident light and a set of sidebands will emerge from the acoustic column as depicted in Figure 2.

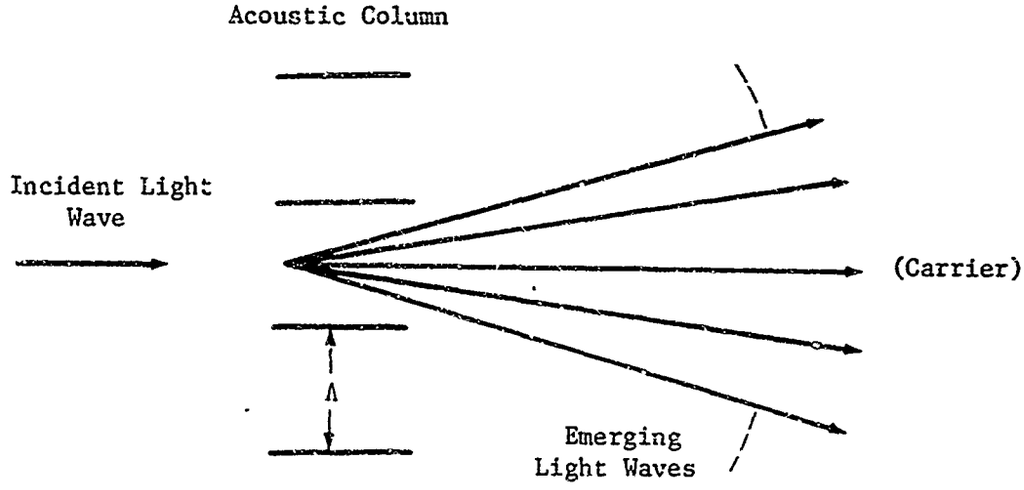

Figure 2. The creation of sidebands caused by frequency modulation on incident plane light wave by a plane acoustic wave train.

The phrase "sufficiently narrow" was used above to describe the width of the acoustic column. The reason for this lies in the fact that the incident light breaks up into its sidebands immediately upon entering the acoustic column and begins to diverge angularly from the carrier. It may then travel through parts of the wave front having different indices of refraction. As a result, destructive interference may occur and the intensity of these bands will be greatly reduced. It is possible to use the interference phenomenon to our advantage by simply impinging the acoustic column with light waves at an angle chosen so that constructive interference will occur.

Bragg Refraction

To describe constructive interference we need to consider Bragg refraction. Bragg's law expresses the condition under which a crystal or any diffraction grating will reflect an incident wave with maximum intensity. Mathematically, the condition is expressed as

$$\sin \theta_B = \frac{N\lambda}{2D} \qquad (2)$$

where

θ_B = Bragg angle

N = integer

D = grating spacing

λ = wavelength of incident wave

Physically, this condition insures that parts of the wavefront which reflect from different strata of the grating are in phase when they recombine. Figure 3 shows schematically the Bragg reflection process when λ is the grating spacing.

As seen in the Figure, the path length difference of the wave which reflects from the top stratum, and the second stratum is $N\lambda$. This insures constructive interference when these waves recombine. Bragg reflection, as described here, is the basis for acousto-optical imaging.

Acousto-Optical Image Formation

Consider a point source of sound, S, from which single frequency acoustic waves are emanating and also a point source of light, O, from which monochromatic light waves are emanating. In the region where the spherical wave fronts of light and sound satisfy the Bragg equation,

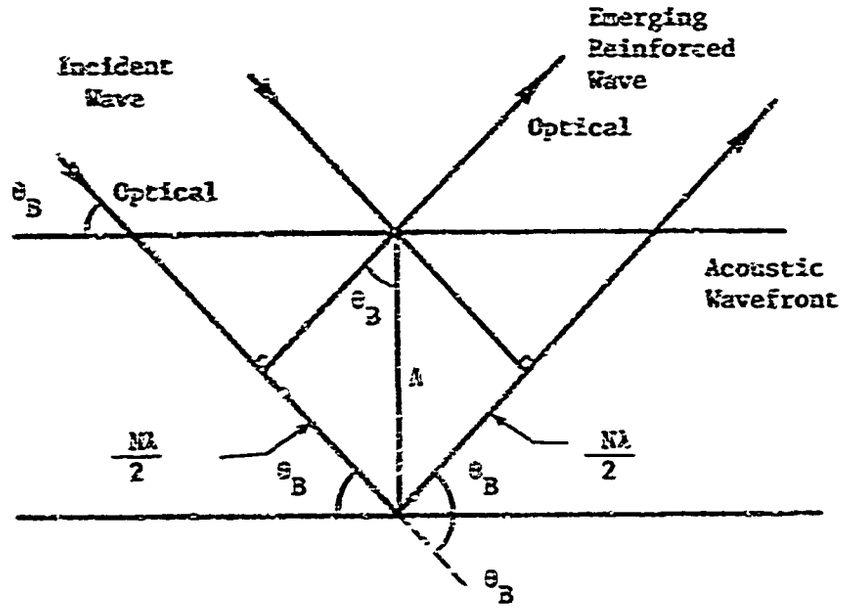

Figure 3. Bragg condition for constructive interference

$\sin \theta_B = \lambda/(2\Lambda)$, maximum reinforcement will occur. If one then traces back these diffracted rays, one finds that they intersect at a single point. Mathematically, this condition is identical to there being a new spherical wave emanating from a point 0'. This point at 0' is then considered to be the virtual image of the sound source, S. Figure 4 depicts this situation for N = 1. Three propagation vectors (→) are shown leaving the light source, 0, which interact with three propagation vectors (⇢) which emanate from the sound source, S, at the Bragg angle θ_B. At these points, diffracted light rays (⇢) are created which when traced back (- - -) intersect at a common point, 0'.

Of course if there were more than one sound source, say S^1, S^2, S^3, ..., then multiple images, $0_1'$, $0_2'$, $0_3'$, ... will be created. Reference 4 shows that a magnification, M, given by

$$M = \frac{\lambda}{\Lambda} \tag{3}$$

will result. For example, if sound sources S^1 and S^2 were separated by a distance S^1S^2, then their images will be separated by a distance

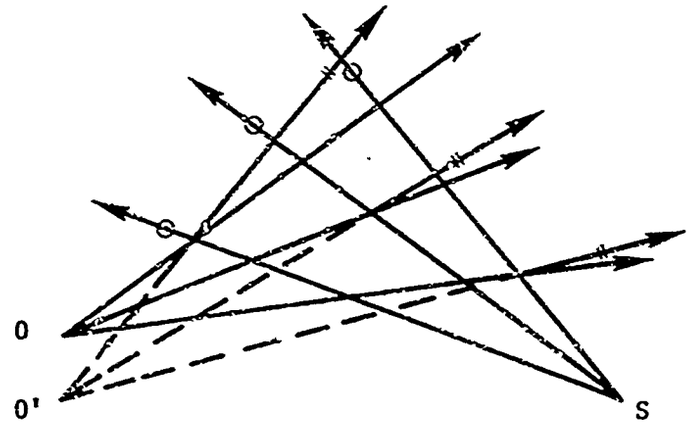

Figure 4. Acousto-Optical Imaging of a sound source, S, by a light source 0, to produce a virtual image 0'.

$(\lambda/A)S^1S^2$. This concept may be generalized to a body merely by considering the body to be made up of many "point" sources, each giving rise to an image. The sum of these images will represent an image of the entire object.

Figure 5 shows a schematic of the apparatus used to form acousto-optical images. The acoustic energy is supplied by an acoustic transducer inserted into a Bragg Cell. The frequency and power output of the transducer is controlled by a variable frequency AC oscillator/amplifier. To provide good acoustic coupling and to minimize acoustic attenuation, the Bragg Cell is filled with a liquid such as water. The optical energy is supplied by a continuous wave laser, such as a Helium-Neon gas laser. The narrow beam of light leaving the laser is expanded by a lens. The spatially diverging light is then collected by a collimating lens and transverses the Bragg Cell, coming to a focus on the other side. A set of lenses near the focal point expands the light projecting it onto a viewing screen. With the transducer turned on, Bragg refraction of the laser light occurs (Fig. 6). The Bragg refracted light spatially diverges from the non-Bragg refracted light. Because of the spatial divergence, the Bragg refracted light becomes projected onto a different portion of the viewing screen than does the non-Bragg refracted light. The image of the Bragg refracted light is of interest in acousto-optical imaging since it contains information regarding the acoustic energy. For convenience, a mask is placed on the optical axis allowing only the Bragg refracted light through. If no object is placed between the acoustic transducer and the light, then the image seen on the viewing screen is that of the transducer alone. Figure 7(a) shows an acousto-optical image of a 1" x 1" transducer oscillating at 8 megacycles. If an object were inserted between the

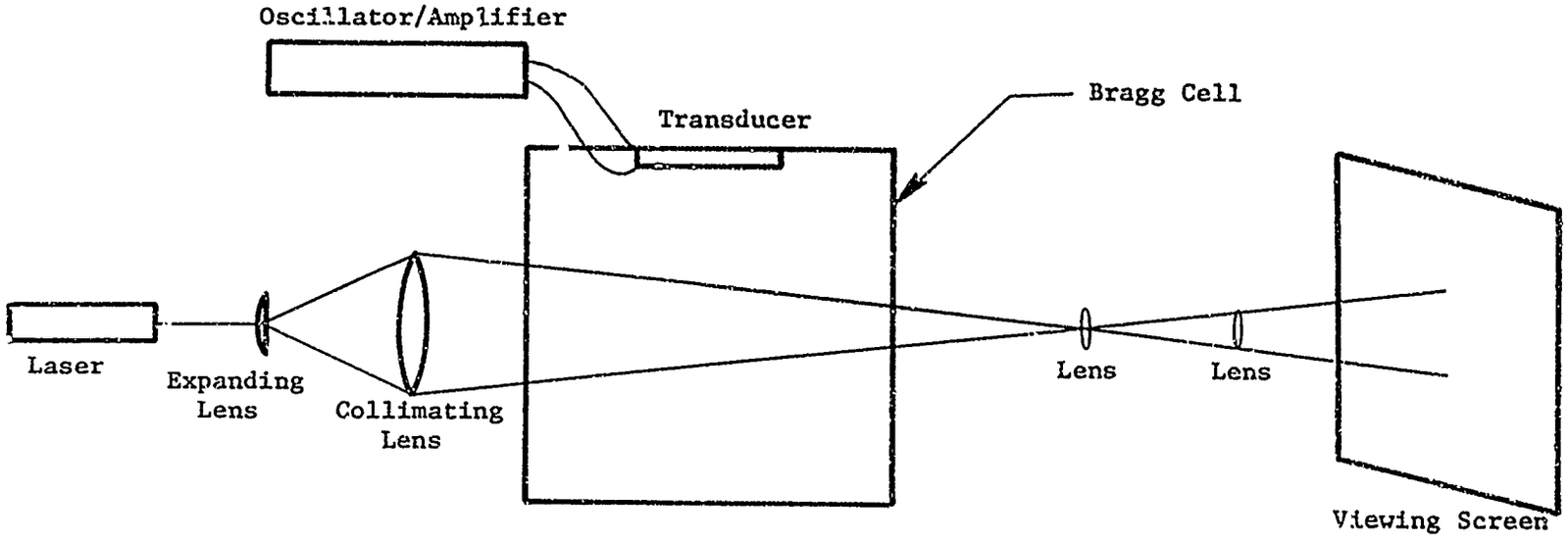

Figure 5 Schematic showing the spatial relationship between the equipment used to obtain acousto-optical images.

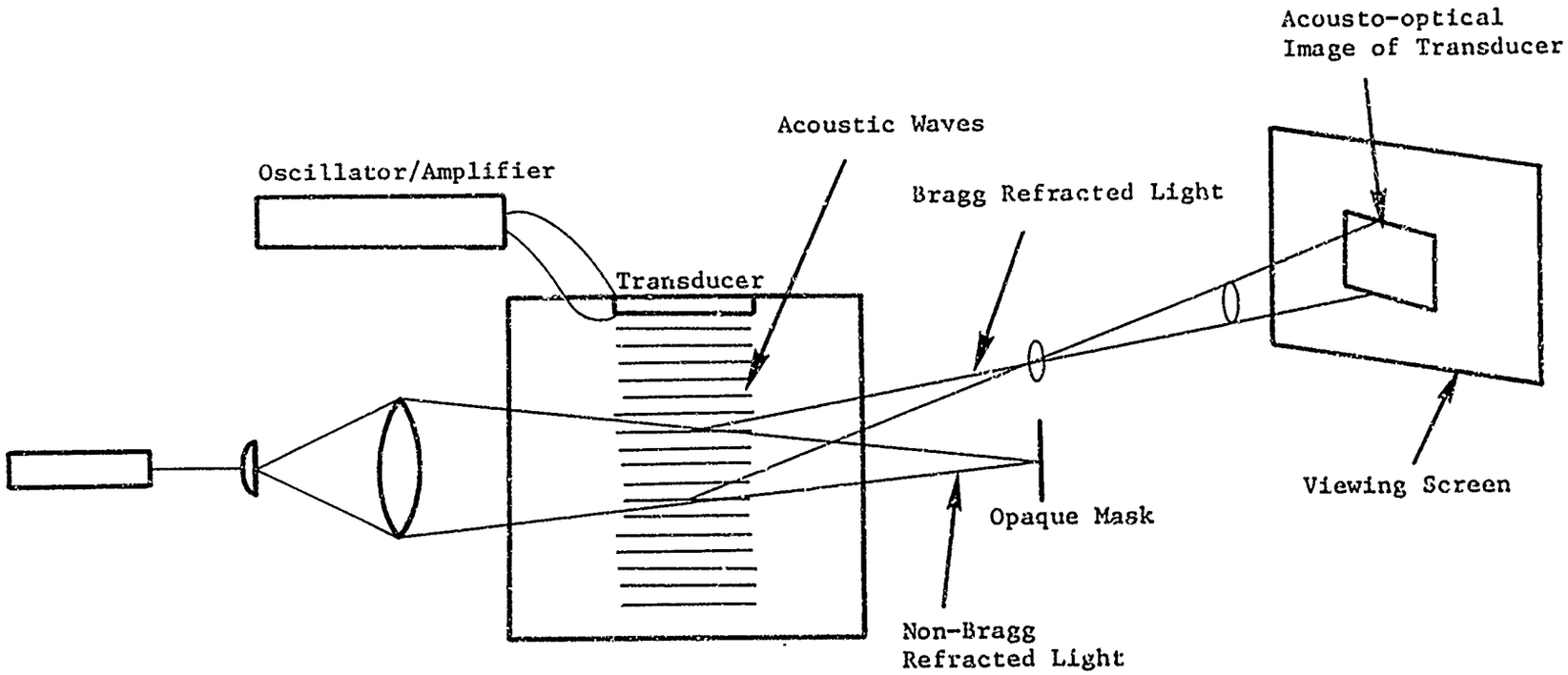

Figure 6 Schematic showing Bragg Refraction of light by acoustic waves.

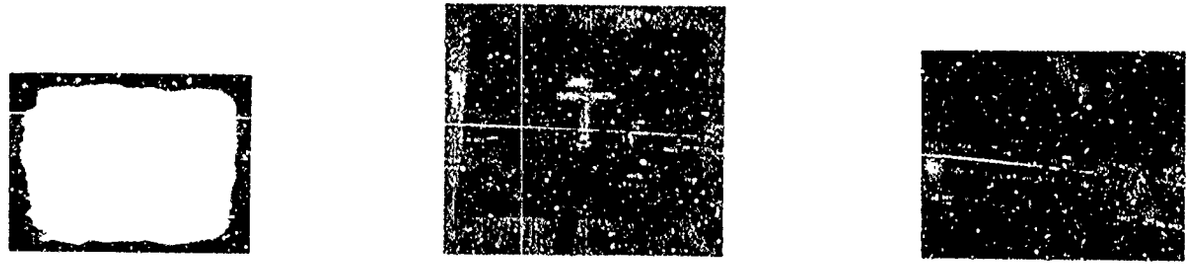

(a) (b) (c)

Figure 7. Demonstration of the Acousto-Optical Imaging Technique

(a) Acousto-optical image of the transducer background
(b) Stencil cutout of the letter "T" which is inserted between the transducer and light cone
(c) Acousto-optical image of the letter "T"

transducer and light cone, the image on the viewing screen will represent the image of the object superimposed on the transducer background. This is demonstrated by inserting a stencil cutout of the letter "T", Figure 7(b) between the transducer and light cone. The cutaway portion of the stencil plate allowed acoustic energy to pass and interact with the light to form the image 7(c). The solid portion of the stencil blocked the sound waves, in turn blackening the transducer background in those regions.

FLAW DETECTION IN 81mm SHELLS

An 81mm shell containing three known flaws was supplied to TRW Systems by the Army Materials & Mechanics Research Center for use in this study. The shell contained two surface flaws (outer surface) and a crack (inner surface). The surface flaws are readily visible by naked eye while the crack is not. The Bragg Cell which was used in this study was not large enough to accommodate the 81mm shell as a single piece. Rather than building a new Bragg Cell, it was decided to section the 81mm into three parts. The sectioned shell (reassembled) is shown in Figure 8. Figure 9 shows the flawed sections individually. Sectioning the shell in this way does not affect the performance of the acousto-optical imaging device. Figure 9(a) shows the segment of the shell containing the crack. The crack is identified schematically by the dotted line. The two surface flaws exist on the outer surface of the shell segment shown in Figures 9(b) and 9(c). The maximum depth of these surface flaws were measured at AMMRC as .005 and .010 inches, respectively.

A special fixture was designed and built to handle the shell in the Bragg Cell of the Acousto-Optical Imaging device. The fixture has the capability of translating and rotating the shell in the Bragg Cell. Figures 10(a) and (b) show one segment of the shell held by the fixture outside and inside of the Bragg Cell, respectively. The capability to both rotate and translate the shell is necessary so that the entire shell case can be conveniently inspected.

Before imaging for flaws, it was necessary to select the proper transducer for this application. Based on previous experience at TRW, flat X-cut quartz crystals were selected. These crystals gave satisfactory performance; therefore no use was made of other shapes, such as cylindrical, which are more expensive, and whose operation is not so well understood. However, to cover a larger frequency range it was necessary to utilize two plane crystals, each having a different fundamental frequency, and operate in their higher harmonics. Crystals having fundamental frequencies of 4 and 8 MHz were selected. The 4 MHz crystal can be operated in higher harmonics to provide acoustic energy at 8, 12, 16, and 20 MHz, while the 8 MHz crystal can operate in its fundamental mode and higher harmonics at 8, 16, and 24 MHz. The two crystals, therefore, provide good coverage of the frequency range from 4 to 24 MHz. These crystals were mounted in an air-backed plexiglas holder. An adhesive (General Electric RTV) was used to firmly affix the crystal in the mounting fixture.

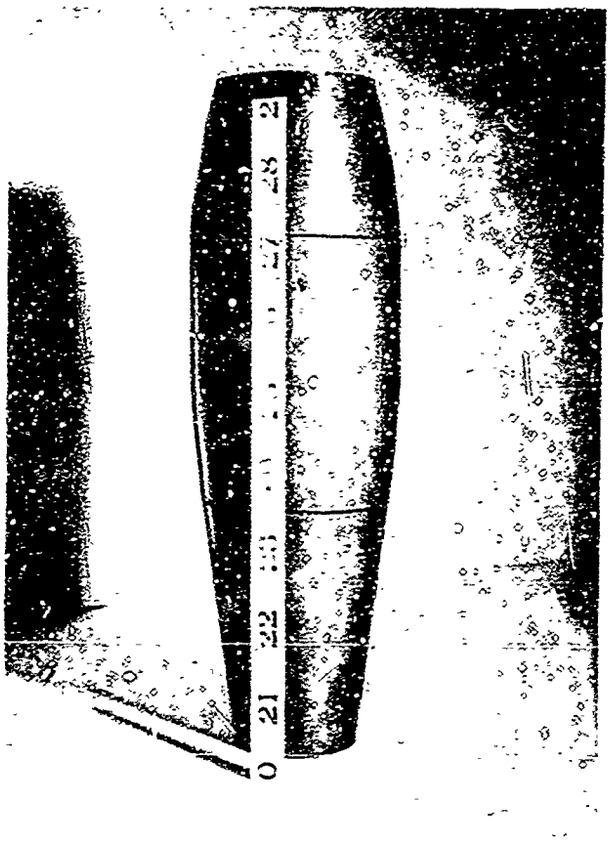

Figure 8 81 mm Shell Known to Contain Two Surface Flaws (Outer Surface) and a Crack (Inner Surface)

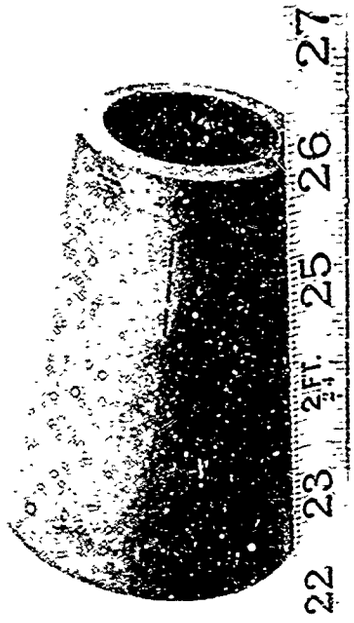

(a)

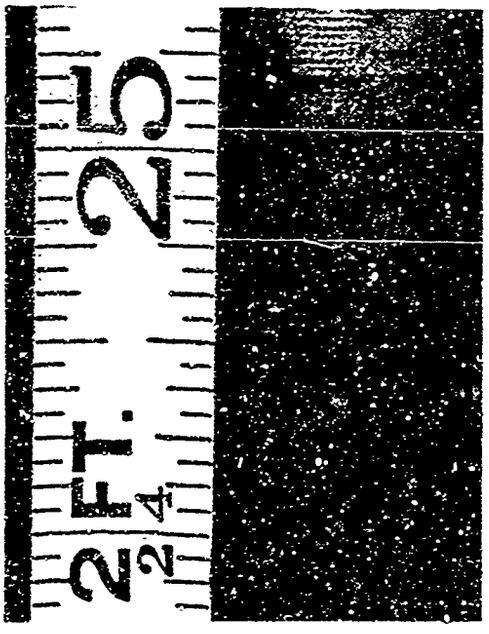

(b)

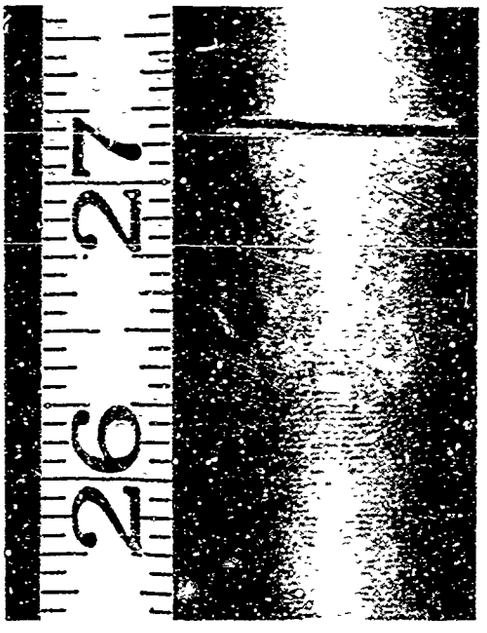

(c)

Figure 9 Sections of the 81 mm Shell Containing the Crack (a) and Two Surface Defects (b) and (c)

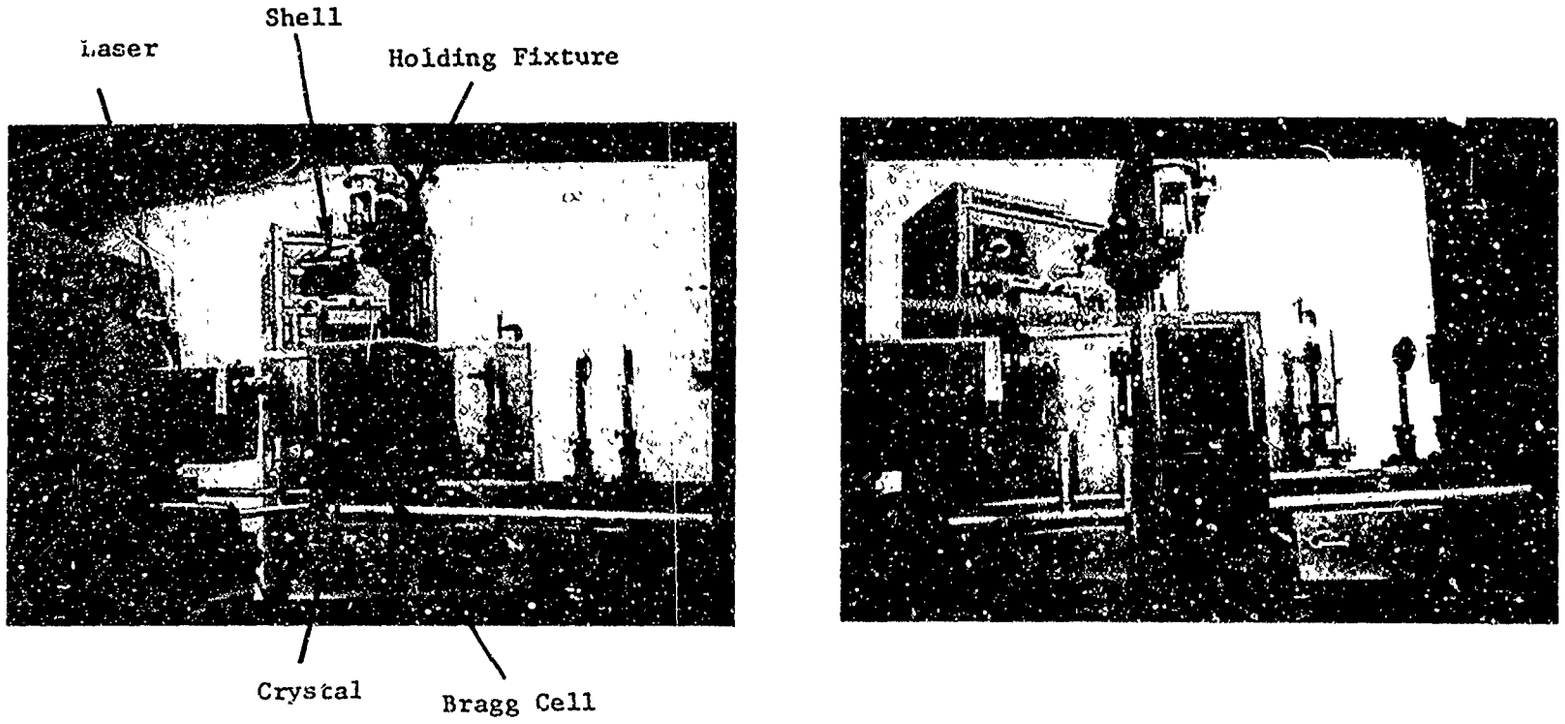

Figure 10 Relationship between the optical axis, acoustic crystal and shell segment.

(a) Shell segment held out of the Bragg Cell.

(b) Shell segment held inside the Bragg Cell.

Test Procedure

The test procedure consisted of inserting the shell segments into the Bragg Cell and visually adjusting its position such that the known flaw was between the transducer and light cone as shown in Figure 11. The light propagates through the center bore of the shell. Sound waves emitted from the transducer propagate through the shell (and flaw) and interact with the light resulting in Bragg refraction. The image of the flaw is then projected onto the viewing screen and recorded by a camera. Beginning with the 4 MHz fundamental crystal operating in its third harmonic, images were obtained of one surface flaw (Figure 9b) at 12 MHz. After the acousto-optical image was recorded by the camera, the oscillator/amplifier was tuned to drive the crystal at 20 MHz (fifth harmonic). The image obtained at that frequency was then recorded by the camera.

The 8 megacycle crystal was then substituted for the 4 MHz crystal. An image of the same flaw was then obtained at 8 and 15 MHz. The inspected segment of the shell was then rotated and the second surface flaw imaged in the same manner. Finally, the segment containing the crack was inserted and acousto-optical images made at 8, 12, 16 and 20 MHz.

Test Results

First Surface Flaw

Figures 12(a), (b) and (c) show the acousto-optical images obtained of the surface flaw shown in Figure 9b at 8, 12 and 16 MHz respectively. The shell segment was inserted into the Bragg Cell by the specially designed fixture and assumed the position shown schematically in Figure 11.

Figure 12(a) was obtained using a 1" x 1-1/2" X-cut crystal operating in its fundamental mode, 8 MHz. The white background represents the crystal background. The flaw is shown as a darkened region in the field of the transducer. Figure 12(b) was obtained using a 1" x 1" X-cut quartz crystal (4 MHz fundamental) operating in its third harmonic (12 MHz). The dark central area represents the surface flaw. Careful examination of Figure 12(b) reveals the presence of faint horizontal lines which were not present in Figure 12(a). They are assumed to be caused by the rough turned machine finish (250 microinch surface roughness). At this higher frequency (12 MHz vs. 8 MHz) the acoustic wavelengths are shorter, resulting in better resolution and making the rough turned machined finish susceptible to imaging. Figure 12(c) was obtained using a 1" x 1-1/2" X-cut quartz crystal (8 MHz fundamental) operating in its second harmonic, 16 MHz. As with the previous two images, the dark area in the field of the transducer background represents the surface flaw. At this higher frequency the rough turned machined finish became more evident.

Second Surface Flaw

Figures 13(a), (b) (c) and (d) show acousto-optical images obtained of the surface flaw shown in Figure 9(c) at 8, 12, 16 and 20 MHz,

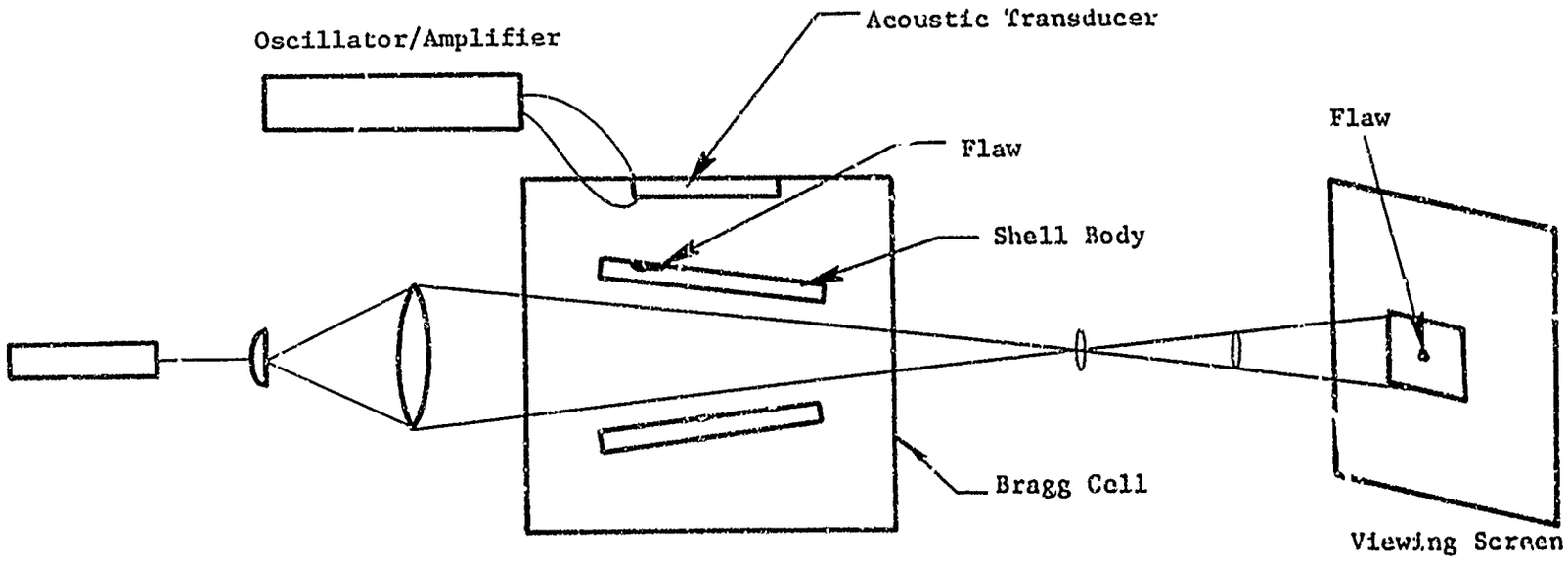

Figure 11 Schematic showing the orientation of the shell casing with respect to the acoustic transducer and laser light.

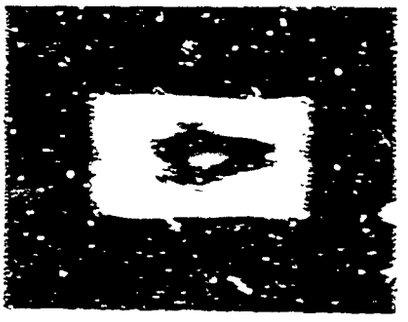

(a)

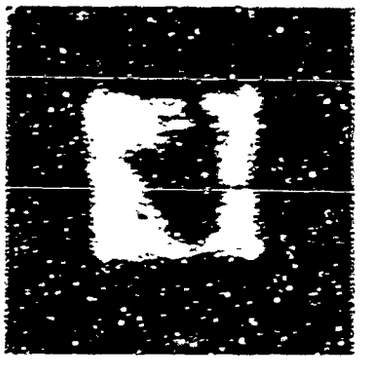

(b)

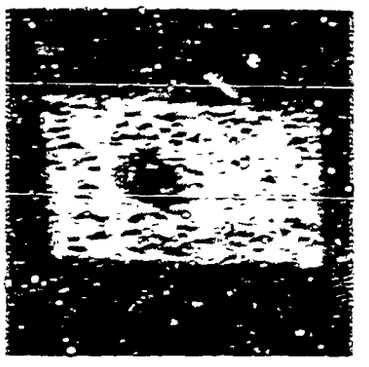

(c)

Figure 12 Acousto-Optical Images of the Surface Flaw Shown in Figure 9(b) Taken at

a) 8 MHz
b) 12 MHz
c) 16 MHz

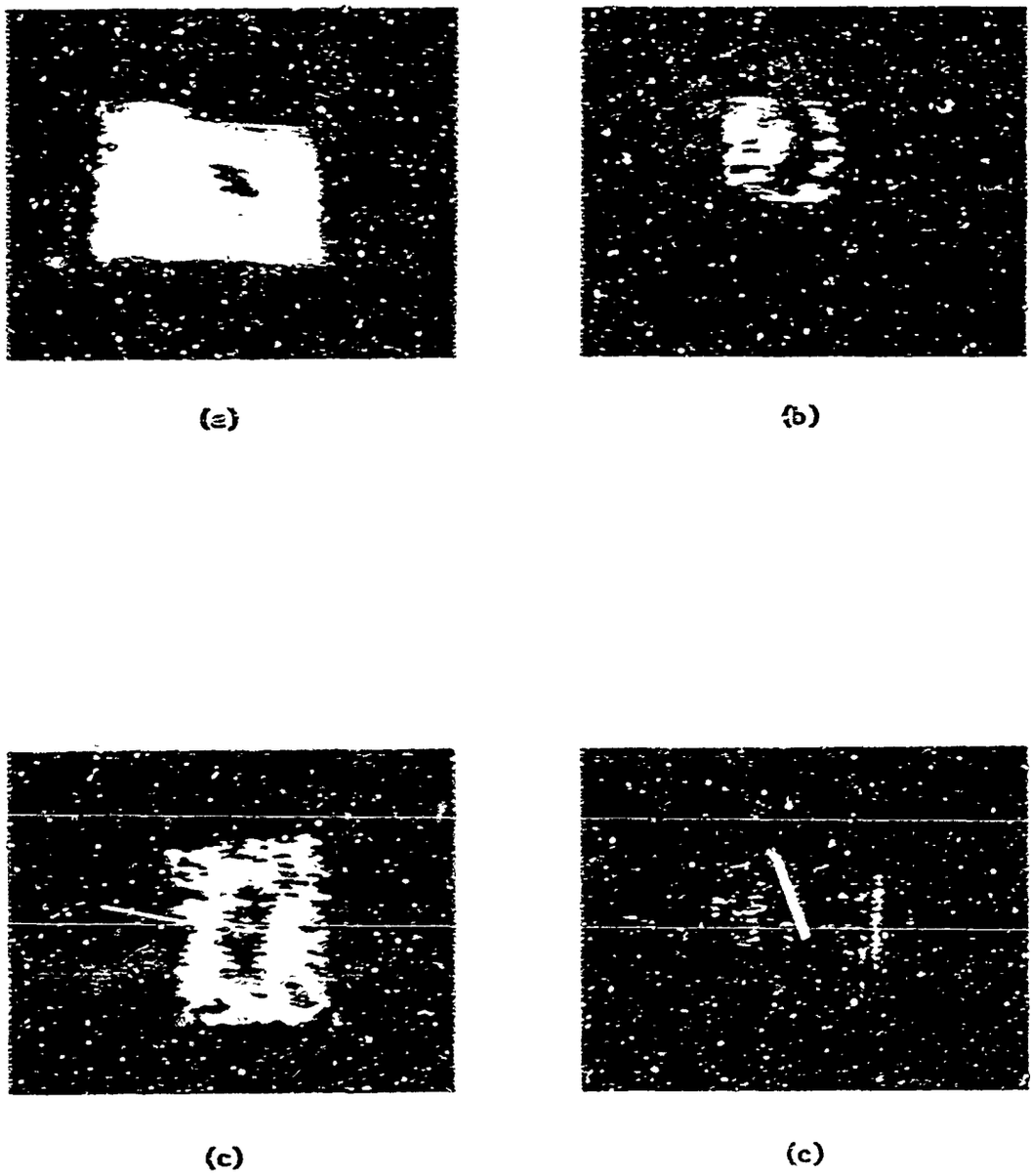

Figure 13. Acousto-optical Images of the Surface Flaw Shown in Figure 9(c) Taken at
(a) 8 MHz
(b) 12 MHz
(c) 16 MHz
(d) 20 MHz

respectively. The section of the shell which contained the flaw was oriented in the Bragg Cell as shown in Figure 11.

Table I summarizes the crystal size and frequency used to obtain the acousto-optical images. Interpretation is identical to that already discussed above.

TABLE I

Figure	Crystal Size	Frequency (MHz)
13(a)	1" x 1-1/2"	8
13(b)	1" x 1"	12
13(c)	1" x 1"	16
13(d)	1" x 1-1/2"	20

Crack Detection

Figures 14(a), (b) and (c) show acousto-optical images of the known crack in the segmented section shown in Figure 9(a). The crack is known to be oriented along the longitudinal axis of the shell. The segment of the shell was placed into the Bragg Cell as shown schematically in Figure 11 with the crack running parallel with the light. Figure 14(a) was obtained using a 1" x 1-1/2" X-cut quartz crystal oscillating in its fundamental mode, 8 MHz. As with the surface flaws, the crack is shown as a darker area in the white background field of the transducer.

Figure 14(b) represents the acousto-optical image of the crack using a 1" x 1-1/2" crystal operating at 16 MHz. The specimen was deliberately rotated in the Bragg Cell so that the crack did not run along the optical axis but rather at an angle to it. The position of the transducer remained the same. This was done deliberately to determine the sensitivity of the alignment of the shell with respect to the transducer and optics. As one can see from Figure 14(b) the crack is still detectable. The internal machining marks are also pronounced at this frequency as they were in the case of the surface flaw studies. Figure 14(c) shows the acousto-optical image obtained of the crack using a 1" x 1-1/2" X-cut quartz crystal operating at 20 MHz. As in the case of the surface flaw studies, the rough turned machined finish became very pronounced at high frequencies. After the acousto-optical images of the crack were made, the 81mm projectile body was sectioned and examined microscopically for determination of both length and depth of the crack in the wall by AMMRC personnel. It was found to have a length of 1-1/4" and a maximum depth of 1/10" or half the wall thickness.

(a)

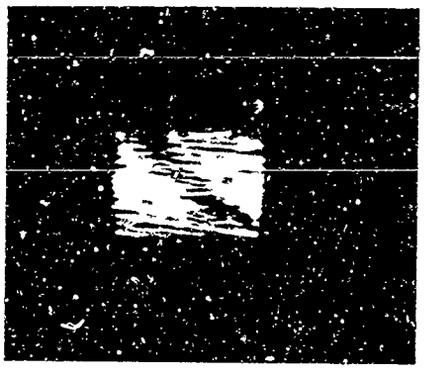

(b)

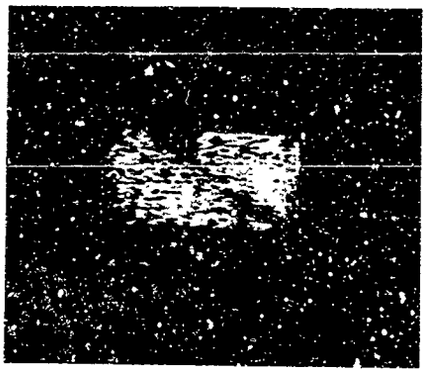

(c)

Figure 14 Acousto-Optical Images of the Crack in Shell Specimen Shown in Figure 9(a) Taken at

a) 8 MHz
b) 16 MHz
c) 20 MHz

In some instances, e.g., when the shell is plugged at one end, one cannot send light through the bore. To show that comparable images may be obtained in these cases a second test procedure was used to obtain an acousto-optical image of the crack. This procedure consisted of inserting the acoustic transducer inside the bore of the projectile body rather than externally as described previously. The experimental setup is shown in Figure 15. One image of the crack was obtained in this manner. The frequency of the acoustic waves was 8 megacycles. The acousto-optical image of the flaw is shown in Figure 16. Comparing Figure 16 with Figure 14(a) shows that the resulting image obtained by this procedure is comparable with having the transducer external to the bore.

Referring to Figure 16, it can be seen that extraneous black lines appear across the face of the transducers. It is felt that these are due to to the nonuniformity of the acoustic beam near its periphery. These lines can be distinguished from the flaw by rotating the shell. In so doing, the image of the flaw moves while these extraneous lines do not.

CONCLUSIONS

The images presented above demonstrate the ability of acousto-optical imaging to depict both surface flaws and cracks in 81mm projectile body casings. At each frequency the acousto-optical images share certain common features. When operating at 8 MHz, the transducer background appears homogeneously white. As the frequency is increased the rough turned machined finish on the projectile become apparent. Judging by these results it appears that 8 MHz is perhaps an optimum choice to avoid distortion and loss of resolution due to the rough turned machined finish.

Surface curvature does not pose a severe problem for this application. It has been expected that the shell, being curved, would effectively form an acoustic lens distorting the optical image. However, this does not appear to be a serious problem, altho gh in some instances some distortion (e.g., Figures 12(b) and 13(c)) is present. The acoustic distortion described above is due to the cylindrical shape of the 81mm projectile body. The effect of cylindrical curvature of the wall on the acoustic waves is similar to the effect of a cylindrical lens to light waves. That is, a distortion only in 1-dimension takes place.

It was also determined that a flat X-cut crystal transducer permits good acousto-optical images of the 81mm shell. This being the case, it is not necessary to go to other shapes. (A cylindrical transducer was considered.) We believe that the foregoing results demonstrate that the acousto-optical imaging device offers Quality Assurance personnel a useful technique for nondestructive testing of projectile body casings.

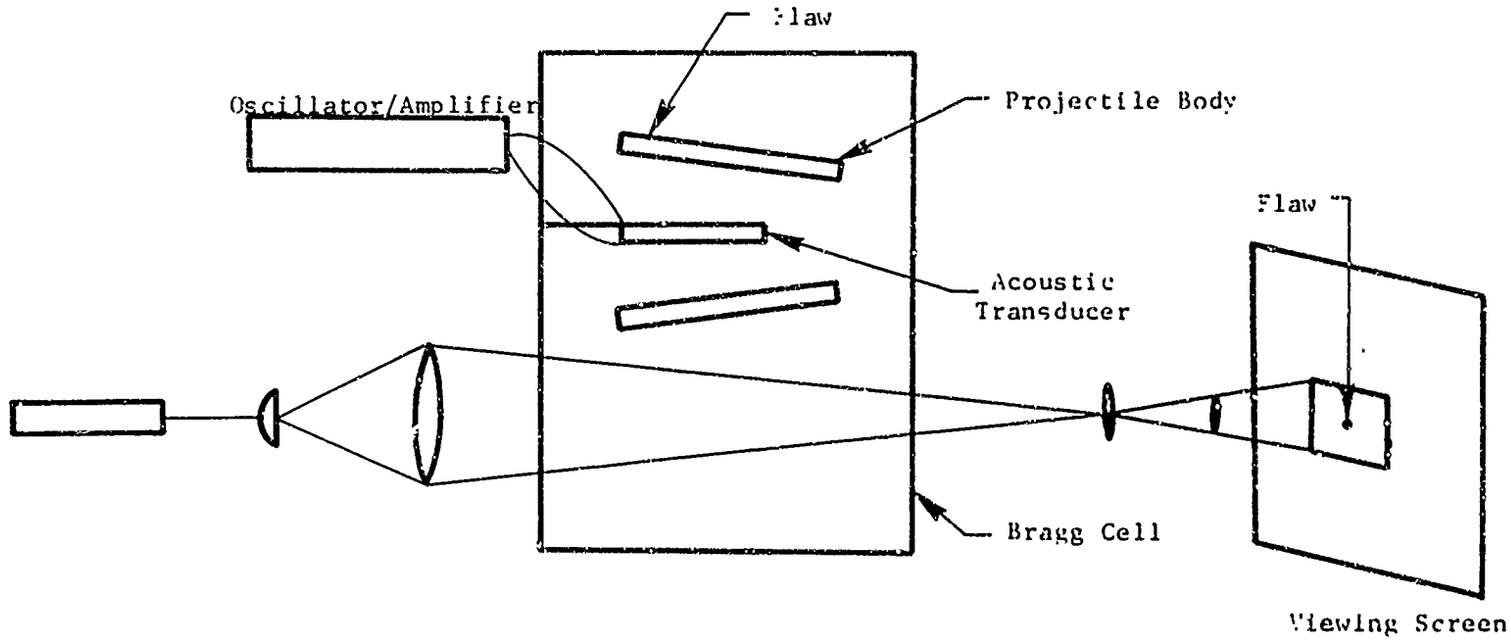

Figure 15 Schematic showing the orientation of the projectile body with respect to the acoustic transducer and laser light when it is not possible to send sound through the bore of the shell.

Figure 16 Acousto-optical image of the crack in the 81mm projectile body. The crystal was placed in the bore of the shell

REFERENCES

1. Brillouin, L., Ann. Phys., (France) Vol. 17, pg. 88 (1922).

2. Debye, P. and Sears, F. W., Proc. Nat. Acad. Sci., (USA), Vol. 18, pg. 409 (1932).

3. Willard, G. W., J. Acoust. Soc. Am., Vol. 21, pg. 101 (1949).

4. Aprahamian, R. and Bhuta, P. G., "TRW Acousto-Optical Imaging Tunnel Detection System," TRW Report 99900-6677-R0-00, July 1968.

ARMY MATERIALS AND MECHANICS RESEARCH CENTER
WATERTOWN, MASSACHUSETTS 02172

TECHNICAL REPORT DISTRIBUTION

No. of Copies	To
20	Commander, Defense Documentation Center, Cameron Station Alexandria, Virginia 22314
30	Director, Army Materials & Mechanics Research Center, Watertown, MA. 02172 ATTN: AMXMR-MQ, Mr. N. Fahey
50	TOTAL COPIES DISTRIBUTED

Unclassified
Security Classification

DOCUMENT CONTROL DATA - R & D

Security classification of title, body of abstract and indexing annotation must be entered when the overall report is classified)

1 ORIGINATING ACTIVITY (Corporate author) TRW INC. TRW Systems Group One Space Park Redondo Beach, California	2a. REPORT SECURITY CLASSIFICATION Unclassified 2b. GROUP

3 REPORT TITLE

DETERMINATION OF FLAWS IN AN 81 MILLIMETER PROJECTILE BODY USING THE TRW ACOUSTO-OPTICAL IMAGING DEVICE

4 DESCRIPTIVE NOTES (Type of report and inclusive dates)

Final Report - 30 January 1970 - 30 July 1970

5 AUTHOR(S) (First name, middle initial, last name)

Robert Aprahamian

6 REPORT DATE	7a. TOTAL NO. OF PAGES	7b. NO. OF REFS
14 August 1970	26	4

8a. CONTRACT OR GRANT NO. DAAG46-70-C-0043 b. PROJECT NO PEMA 15042 c. AMCMS Code 4931.0M.5042 d.	9a. ORIGINATOR'S REPORT NUMBER(S) AMMRC CR 70-20 9b. OTHER REPORT NO(S) (Any other numbers that may be assigned this report)

10 DISTRIBUTION STATEMENT

This document has been approved for public release and sale; its distribution is unlimited.

11 SUPPLEMENTARY NOTES	12. SPONSORING MILITARY ACTIVITY
	Army Materials and Mechanics Research Center, Watertown, Massachusetts 02172

13 ABSTRACT

This report contains the results of a six month study designed to establish the applicability of the TRW Acousto-Optical Imaging System in depicting internal defects and surface flaws existing in an 81mm projectile body. An 81mm projectile body was furnished to TRW Systems which contained three known flaws. The known flaws consisted of two surface flaws on the outer surface of the shell and one crack in the inner wall. Acousto-optical images of these three flaws were obtained in the frequency range from 8 to 20 megacycles.

DD FORM 1 NOV 68 1473 REPLACES DD FORM 1473, 1 JAN 64, WHICH IS OBSOLETE FOR ARMY USE.

Unclassified
Security Classification

14 KEY WORDS	LINK A		LINK B		LINK C	
	ROLE	WT	ROLE	WT	ROLE	WT
Nondestructive Testing						
Ultrasonic Tests						
Acoustics						
Images						
Cylindrical Shells						
Projectiles						